Globally exponentially stable filters for underwater position estimation using an array of hydroacoustic transducers on the vehicle and a single transponder

Bård N. Stovner [a,*], Tor A. Johansen [b], Ingrid Schjølberg [a]

[a] Department of Marine Technology, University of Science and Technology (NTNU), 7491 Trondheim, Norway
[b] Department of Engineering Cybernetics, NTNU, 7491 Trondheim, Norway

A B S T R A C T

This paper presents two novel globally exponentially stable position estimators using hydroacoustic measurements from a single transponder to several transceivers on the vehicle. A comparison study of these and several existing filters is conducted with both experimental and simulated data. Two classes of filters for position estimation are compared: filters expressing the position of an underwater vehicle in the body-fixed and north-east-down coordinate frames. The comparison study showed that the latter formulation yields lower estimation errors. Furthermore, one of the novel filters developed in this paper using the north-east-down formulation is found to serve well as a compromise between performance, theoretical stability, and computational complexity relative to the near-optimal linearization-based filters with which it is compared.

1. Introduction

Current subsea inspection, maintenance, and repair (IMR) operations are heavily dependent on manually operated remotely operated vehicles (ROVs). This is time-consuming and expensive as it requires deployment of a surface vessel and experienced personnel, Schjølberg et al. (2016). Increased autonomy in current ROV operations may make current operations more efficient, while being a stepping-stone towards future solution that e.g. are independent of the expensive surface vessel. This paper considers inertial navigation of an (UV) in areas of little interest, e.g. in transit between subsea facilities.

Inertial navigation of an underwater vehicle (UV) commonly involves two steps. One is the integration of rate measurements in order to update position and attitude estimates. These measurements are often provided by accelerometers or Doppler velocity log (DVL) for position estimation and angular rate sensor (ARS) for attitude estimation. Due to the noisy and biased nature of inertial measurements, the integration causes the position and attitude estimates to drift over time. Therefore, a second step is needed, namely aiding the inertial navigation using absolute measurements of position and attitude. The absolute measurement for attitude estimation is often provided by on-board sensors such as accelerometers and magnetometers or compasses. These provide body-fixed measurements of known reference vectors in the global frame, and

from this, the rotation between the body-fixed and global frame can be calculated. For underwater position estimation, these absolute measurements often come from hydroacoustic networks providing range measurements from known locations. Most commonly used is the long baseline (LBL) network in which several transducers are mounted on the sea-bed and one transducer is carried by the vehicle. The short baseline (SBL) has a similar structure, except the array of transducers are mounted under a surface vessel, from which the UV with one transducer is often employed. In ultrashort baseline (USBL) systems, the array of transducers are compactly fitted inside an apparatus that is mounted under a surface vessel. The baselines, i.e. the geometry of transducers, impact the position estimation accuracy, where longer distances and more diversity generally yield higher estimation accuracy. For an overview of these set ups, we refer to Vickery (1998). These acoustic set ups also exist in slightly modified configurations. The GPS intelligent buoy (GIB) network is similar to LBL, only that the transducers are mounted to global positioning system (GPS) positioned buoys. In inverted ultrashort baseline (iUSBL), the USBL apparatus is mounted on the UV. Lastly, Stovner and Johansen (2017) suggested an inverted short baseline (iSBL) set up in which transducers are spaced out as widely as possible on the UV. This gives a similar set up as the iUSBL, but the baselines are now confined to the size of the UV instead of a small apparatus. This set up is depicted in Fig. 1.

---

* Corresponding author.
E-mail addresses: bard.b.stovner@ntnu.no (B.N. Stovner), tor.a.johansen@itk.ntnu.no (T.A. Johansen), ingrid.schjolberg@ntnu.no (I. Schjølberg).
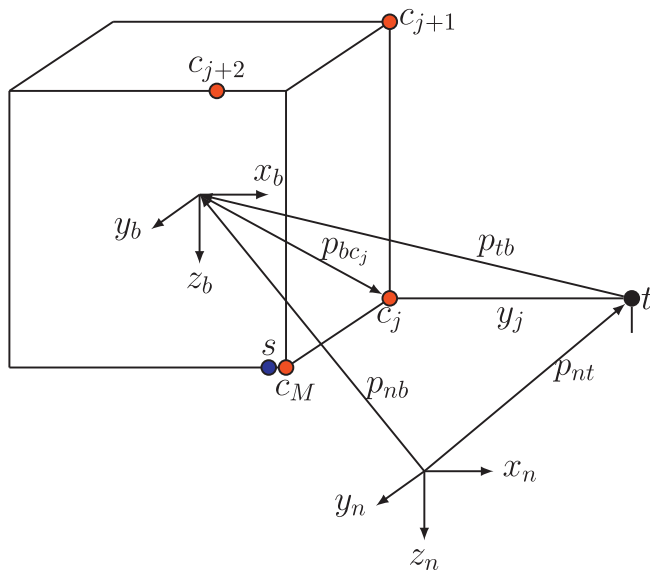
Fig. 1. The iSBL set up with a sender s (blue) and receivers c_j (red) mounted on an UV, and a transponder t on the seabed (black). (For interpretation of the references to color in this figure legend, the reader is referred to the Web version of this article.)

The advantage of both iSBL and iUSBL compared to e.g. LBL is the lower requirement for external infrastructure. Assuming an attitude estimate is available, iSBL and iUSBL only needs contact with one transponder in order to find its global position, whereas with LBL, three transponders are typically needed. In areas of little interest, e.g. in transit between subsea facilities, it is desirable to install as little infrastructure as possible, both to save deployment and maintenance costs. The trade-off of navigation precision for less infrastructure is not critical in these areas.

Due to longer baselines, iSBL is potentially more accurate than iUSBL. Also, one can use cheap light-weight transducer elements instead of a relatively expensive, heavy, and large USBL apparatus. This is especially important for small light-weight UVs. Morgado et al. (2011a, b); Batista et al. (2014) developed Kalman filters (KFs) with global stability properties using a linear model achieved through state augmentation for iUSBL measurements. There, the range and range-difference measurements were used in a tightly-coupled scheme, and not used to calculate a position measurement or range and bearing measurements as is common with USBL sensors. Also, the receiver baselines on the vehicle are larger than one would typically expect from a USBL apparatus, i.e. they spanned $20 \times 30 \times 30 cm$. Therefore, the proposed hydroacoustic set up in Morgado et al. (2011a) has many similarities with the measurement set up used in this paper. Morgado et al. (2013) presented an extended Kalman filter (EKF)-based solution for the same measurement set up, where the full state, i.e. position, velocity, and attitude along with ARS and accelerometer biases, was estimated.

Another set up that requires only one transponder exists, in which only one transceiver on the vehicle is assumed as well. This estimation problem is not observable in each instant, but can be shown to be observable over time for sufficiently rich vehicle movements, as shown by Batista et al. (2010) for a state augmentation based solution to the nonlinear estimation problem. Several EKF- and particle filter (PF)-based solutions have also been developed, see e.g. Ferreira et al. (2010); Saúde and Aguiar (2009).

The EKF is the workhorse for estimation of nonlinear systems. It linearizes the nonlinear model about its own estimate, and employs the linearized model in a linear KF. However, the feedback of the state estimate as a linearization point is potentially destabilizing. This has inspired solutions where a linear model is achieved without the need for the feedback of the state estimate. Batista et al. (2012) and Morgado et al. (2011a) find a linear model by algebraic manipulation of the

measurement equations, thus avoiding the feedback of a linearization point. Furthermore, they are able to show global stability properties. Another way of linearizing the nonlinear model while avoiding the feedback of a linearization point is to linearize about an exogenous state estimate which has desired stability properties, but may be suboptimal. This is the idea of the exogenous Kalman filter (XKF) of Johansen and Fossen (2017). A special case of the XKF is the three-stage filter (3SF) of Johansen et al. (2016) where the linearization point is provided by a cascade of an algebraic transformation that supplies a linear model to a suboptimal but globally asymptotically stable KF. The algebraic transformation stage is generally similar to that in Bancroft (1985) and Chaffee and Abel (1994). Stovner et al. (2016) developed a 3SF for underwater position estimation using an LBL network, which Jørgensen et al. (2016) improved upon by a more accurate model of the noise. In Stovner et al. (2017) the 3SF was used for body-fixed position estimation with an iSBL network, and Stovner and Johansen (2017) extended the work to aid attitude estimation in the case of unreliable magnetometer measurements.

The presented work contains several contributions. The 3SFs of Stovner et al. (2017) are improved upon by using a novel algebraic transformation inspired by Morgado et al. (2011a). The novel algebraic transformation produces a linear time-varying (LTV) measurement model where the original range and range difference measurements are still used as measurements. This is contrary to Batista et al. (2012), where a position was calculated and used as measurement; Morgado et al. (2011a, b) and Batista et al. (2014), where state augmentation was used to handle nonlinear terms; and Stovner et al. (2017), where the algebraic transformation constructed new measurements that drastically increased the effect of measurement noise. The novel filters, which essentially are improvements on those of Stovner et al. (2017), express the state both in the body-fixed and northeast-down (NED) coordinate frames. These are thoroughly developed and shown to have global exponential stability (GES) error dynamics.

The filters are compared both in simulations and experimentally to Stovner et al. (2017), a loosely coupled filter, and a standard EKF implementation. The second stage LTV KFs using the NED formulation is shown to outperform the second stage filters of Stovner et al. (2017). In fact, it is shown to yield nearly as good performance as the third stage filter based on the linearized model. Therefore, with a minor reduction in estimation precision, one can reduce the computational burden by half relative to the 3SF presented in Stovner et al. (2017).

The contributions are summarized below:

- Two novel three-stage filter for underwater position estimation are developed and proven to have global exponential stability error dynamics. This comes with robustness guarantees, especially with regards to the transient behavior.
- The filters are verified in simulations and experiments, and calculated mean absolute error values show that EKF-like performance is achieved.

2. Preliminaries

On the UV, there is one transmitting and M receiving hydroacoustic transducer elements denoted the *sender* and *receivers*, respectively. In the vehicle's surroundings, a *transponder* is placed, capable of both receiving and transmitting. This set up is depicted in Fig. 1.

Let p_{bc}^a denote the position of point c relative to point b decomposed in the coordinate frame a. In the case where c or b generally denote a coordinate frame, the point is the origin of the respective frame. Now, $p_{bc_j}^b$ and p_{tb}^b denotes the position of receiver c_j relative to the vehicle and the vehicle relative the transponder t, respectively, both decomposed in the body-fixed frame. p_{nb}^n and p_{nt}^n denotes the position of the vehicle and transponder relative to the origin of the local NED frame, respectively, both decomposed in the NED frame. Similarly, the ground velocity of the

vehicle decomposed in the body-fixed and NED frames is v_{nb}^b and v_{nb}^n, respectively. Now, we define the body-fixed and NED state vectors as

$$x \triangleq \begin{bmatrix} p_{tb}^b \\ v_{nb}^b \end{bmatrix}, \quad \chi \triangleq \begin{bmatrix} p_{nb}^n \\ v_{nb}^n \end{bmatrix} \tag{1}$$

respectively. Denote the rotation from the body-fixed to NED frame as R_b^n. In this paper, the ARS measurements are assumed to be biased, and the ARS bias b^b is assumed estimated by an attitude estimator. Now, we define the attitude state tuple $z \triangleq (R_b^n, b^b)$. For $z_1 = (R_1, b_1)$ and $z_2 = (R_2, b_2)$, we define the notation $z_1 - z_2 = (R_1 - R_2, b_1 - b_2)$. Also, $\|z_1\|^2 = \|R_1\|^2 + \|b_1\|^2$.

3. Modeling

3.1. Measurement model

The Euclidean distance between transponder t and receiver c_j is described by

$$\rho_j = \left\| p_{tb}^b + p_{bc_j}^b \right\| \tag{2a}$$

$$= \left\| p_{nb}^n - p_{nt}^n + R_b^n p_{bc_j}^b \right\| \tag{2b}$$

where $\| \cdot \|$ denotes the Euclidean norm. Assume the sender is mounted next to receiver c_M, which is responsible for contacting the transponder. Further assume that the vehicle moves slowly relative to the speed of sound. The time-of-arrival (TOA) detected by c_M measures the distance from sender to transponder and back in addition to noise: $2\rho_M + \varepsilon_y + \varepsilon_{\partial,M}$. Therefore, we model the range measurement y_M by

$$y_M = h_M(x) \triangleq \rho_M + \frac{1}{2}\varepsilon_y + \frac{1}{2}\varepsilon_{\partial,M} \tag{3}$$

where $\varepsilon_y \sim \mathcal{N}(0, \sigma_y^2)$ is noise on the range measurement and $\varepsilon_{\partial j} \sim \mathcal{N}(0, \sigma_\partial^2), j \in (1, ..., M)$ is a noise term unique for receiver c_j. The time-difference-of-arrival (TDOA) measured at receiver c_j for $j \in (1, ..., M-1)$ is described by

$$\delta y_j = h_j(x) \triangleq \rho_j - \rho_M + \varepsilon_{\partial,j} - \varepsilon_{\partial,m} \tag{4}$$

We define the measurement and measurement model vectors

$$y \triangleq \begin{bmatrix} \delta y_1 & \cdots & \delta y_{M-1} & y_M \end{bmatrix}^\top$$
$$h(x) \triangleq \begin{bmatrix} h_1(x) & \cdots & h_{M-1}(x) & h_M(x) \end{bmatrix}^\top$$

Also, we notice that $h(x) \equiv h(\chi, z)$, where $h(\chi, z)$ is the concatenation of (4) and (3) inserted with (2).

The ARS and accelerometer measurements are modeled by

$$\omega_{nb,m}^b = \omega_{nb}^b + b^b + \varepsilon_{ars} \tag{5}$$

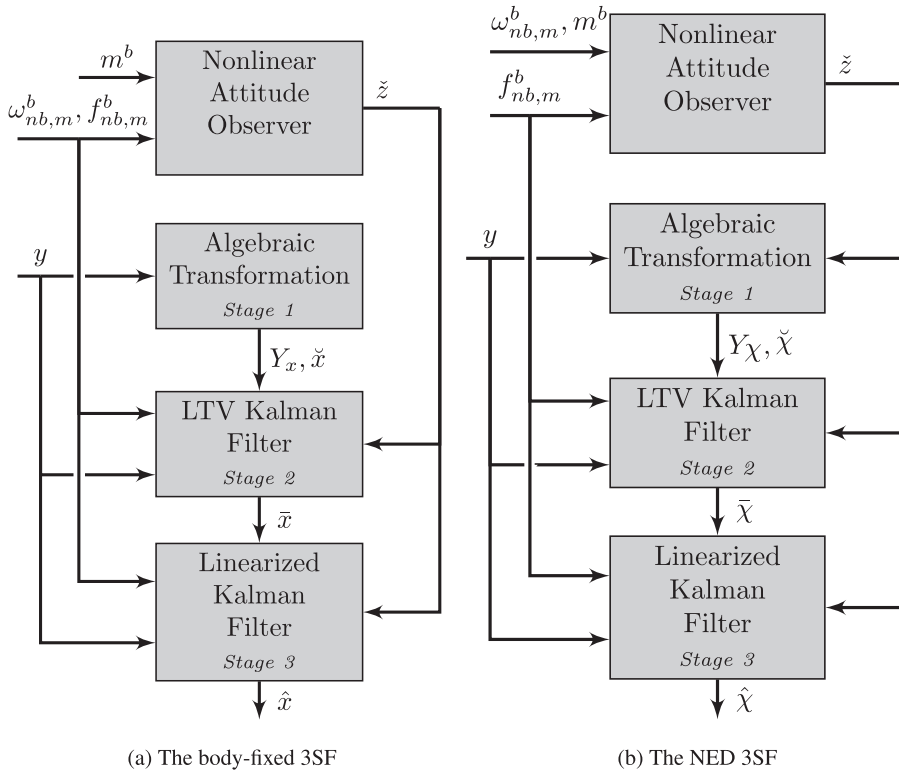$$f_{nb,m}^b = a_{nb}^b - R^\top(q_b^n)g^n + \varepsilon_{acc} \tag{6}$$

respectively, where ω_{nb}^b, b^b, g^n, and a_{nb}^b are the angular rate, ARS bias, gravity vector and the acceleration, respectively. The accelerometer and ARS noise terms are described by $\varepsilon_{ars} \sim \mathcal{N}(0, \sigma_{ars}^2)$ and $\varepsilon_{acc} \sim \mathcal{N}(0, \sigma_{acc}^2)$, respectively. Note the implicit assumption that the origin of the body-fixed frame coincides with the inertial measurement unit (IMU). If this is not the case, the accelerometer measurements would be more appropriately modeled by

$$f_{nI,m}^b = a_{nb}^b + S^2(\omega_{nI}^b)p_{Ib}^b + S(\dot{\omega}_{nI}^b)p_{Ib}^b - R^\top(q_b^n)g^n + \varepsilon_{acc},$$

where $\{I\}$ denotes the body-fixed frame centered in the IMU. Here, one could either assume that p_{Ib}^b or ω_{nI}^b and $\dot{\omega}_{nI}^b$ are small enough that the Coriolis terms are negligible, or subtract estimates of the Coriolis terms to cancel them out.

The normalized magnetometer measurement vector m^b is modeled by $m^b = R_b^{n\top}m^n + \varepsilon_{mag}$ where m^n is a known NED reference vector at the

(a) The body-fixed 3SF

(b) The NED 3SF

Fig. 2. The structure of the 3SF for the body-fixed and NED formulations.

location and the magnetometer noise is $\varepsilon_{mag} \sim \mathcal{N}(0, \sigma_{mag}^2)$.

3.2. Kinematic model

The kinematics of R_b^n and b_{ars}^b are

$$\dot{R}_b^n = R_b^n S(\omega_{nb}^b) \tag{7a}$$

$$\dot{b}_{ars}^b = 0 \tag{7b}$$

where $S(\cdot)$ is the skew-symmetric matrix

$$S(\omega) = \begin{bmatrix} 0 & -\omega_3 & \omega_2 \\ \omega_3 & 0 & -\omega_1 \\ -\omega_2 & \omega_1 & 0 \end{bmatrix}, \omega = \begin{bmatrix} \omega_1 \\ \omega_2 \\ \omega_3 \end{bmatrix}$$

The kinematics of the body-fixed translational motion state is

$$\dot{p}_{tb}^b = -S(\omega_{nb}^b)p_{tb}^b + v_{nb}^b \tag{8a}$$

$$\dot{v}_{nb}^b = -S(\omega_{nb}^b)v_{nb}^b + a_{nb}^b \tag{8b}$$

Inserting (5)–(6) into (8) and writing it in matrix form yields

$$\dot{x} = A_x(t,z)x + B_x(z)u + G_x(x)\varepsilon_x \tag{9}$$

where

$$A_x(t,z) = \begin{bmatrix} -S\left(\omega_{nb,m}^b - b^b\right) & I_3 \\ 0_{3\times3} & -S\left(\omega_{nb,m}^b - b^b\right) \end{bmatrix}$$

$$B_x(z) = \begin{bmatrix} 0_{3\times3} & 0_{3\times3} \\ I_3 & R_b^{n\top} \end{bmatrix}, \quad u(t) = \begin{bmatrix} f_{acc}^b \\ g^n \end{bmatrix}$$

$$G_x(x) = \begin{bmatrix} -S(p_{tb}^b) & 0_{3\times3} \\ -S(v_{nb}^b) & -I_3 \end{bmatrix}, \quad \varepsilon_x = \begin{bmatrix} \varepsilon_{ars} \\ \varepsilon_{acc} \end{bmatrix}$$

The kinematics of the NED translational motion state is

$$\dot{p}_{nb}^n = v_{nb}^n \tag{10a}$$

$$\dot{v}_{nb}^n = a_{nb}^n \tag{10b}$$

Inserting (6) into (11) yields

$$\dot{\chi} = A_\chi \chi + B_\chi(z)u + G_\chi \varepsilon_\chi \tag{11}$$

$$A_\chi = \begin{bmatrix} 0 & I \\ 0 & 0 \end{bmatrix}, B_\chi(z) = \begin{bmatrix} 0 & 0 \\ R_b^n & I \end{bmatrix}$$

$$G_\chi(z) = \begin{bmatrix} 0 \\ R_b^n \end{bmatrix}, \varepsilon_\chi = \varepsilon_{acc}$$

4. Filter development

In this section, 3SFs using body-fixed and NED model formulations are developed and their error dynamics are derived. The 3SFs consist of an attitude observer and three stages of position estimation. The first stage, described in Section 4.2, is an algebraic transformation that algebraically linearizes the nonlinear measurement model. The second stage is a KF using the algebraically transformed LTV model, and is described in Section 4.3. In Section 4.4, the third stage is described, in which the nonlinear model is linearized about the estimate from the second stage. The general structure of the body-fixed and NED formulations are depicted in Fig. 2.

Before deriving the estimators, two key assumptions are stated.

Assumption 1. There are at least two nonparallel reference vectors.

Assumption 2. There are at least four non-coplanar receivers on the UV.

4.1. Attitude observer

The nonlinear attitude observer from Grip et al. (2015) is used, which outputs the rotation matrix estimate R_b^n and ARS bias estimate $\hat{b}^b$. Define the tuple $\check{z} \triangleq (R_b^n, \check{b}^b)$ and the corresponding estimation error $\tilde{z} = z - \check{z}$. Denote by $\Sigma_{\tilde{z}}$ the dynamics of the estimation error $\tilde{z}$.

Proposition 1 *Suppose* Assumption 1 *is satisfied. Then, the origin* $\tilde{z} = (0,0)$ *of* $\Sigma_{\tilde{z}}$ *is GES.*

Proof. The proof follows from Grip et al. (2015).

4.2. Stage 1: algebraic transformation

4.2.1. Body-fixed algebraic transformation
We begin by computing, in the noise-free case,

$$\rho_j^2 - \rho_M^2 = (\rho_j - \rho_M)(\rho_j + \rho_M) = 2\left(p_{bc_j}^b - p_{bc_M}^b\right)^\top p_{tb}^b + \left\|p_{bc_j}^b\right\|^2 - \left\|p_{bc_M}^b\right\|^2$$

Inspired by Batista et al. (2012), we write

$$\rho_j - \rho_M - \frac{\left\|p_{bc_j}^b\right\|^2 - \left\|p_{bc_M}^b\right\|^2}{\rho_j + \rho_M} = 2\frac{\left(p_{bc_j}^b - p_{bc_M}^b\right)^\top}{\rho_j + \rho_M}p_{tb}^b$$

and insert δy_j for $\rho_j - \rho_M$ and $\delta y_j + 2y_M$ for $\rho_j + \rho_M$ to obtain

$$Y_x' = \begin{bmatrix} \delta y_1 + \nu_{x,1} \\ \vdots \\ \delta y_{M-1} + \nu_{x,M-1} \end{bmatrix} = \underbrace{\begin{bmatrix} C_{x,1} \\ \vdots \\ C_{x,M-1} \end{bmatrix}}_{C_{x,p}'} p_{tb}^b \tag{12}$$

where

$$\nu_{x,j} = -\frac{\left\|p_{bc_j}^b\right\|^2 - \left\|p_{bc_M}^b\right\|^2}{\delta y_j + 2y_M}, C_{x,j} = 2\frac{\left(p_{bc_j}^b - p_{bc_M}^b\right)^\top}{\delta y_j + 2y_M} \tag{13}$$

In the measurement model (12), the $M-1$ range difference measurements are used. In order to use the Mth measurement, i.e. the range measurement between the sender and transponder, we use (12) to calculate a crude estimate of p_{tb}^b about which we linearize (3):

$$\check{p}_{tb}^b = C_{x,p}'^\dagger Y_x'$$

Now, we define $\check{x} = [\check{p}_{tb}^n; 0_{3\times1}]$ and Taylor expand (3)

$$h_M(x) = h_M(\check{x}) + H_{x,M}(\check{x})(x - \check{x}) + \overline{\varphi}_{x,M}\left(p_{tb}^b - \check{p}_{tb}^b\right)$$

where $\overline{\varphi}_{x,M}(p_{tb}^b - \check{p}_{tb}^b)$ are higher order terms, $\overline{\varphi}_{x,M}(0) = 0$, and

$$H_{x,M}(\check{x}) = \frac{dh_M(x)}{dx}\bigg|_{x=\check{x}} = \begin{bmatrix} \frac{\left(\check{p}_{tb}^b - p_{bc_M}^b\right)^\top}{\left\|\check{p}_{tb}^b - p_{bc_M}^b\right\|} & 0_{1\times3} \end{bmatrix} \tag{14}$$

Finally, we define $C_x' \triangleq [C_{x,p}', 0_{M-1\times3}]$, $C_x \triangleq [C_x'; H_{x,M}(\check{x})]$, and $Y_x \triangleq [Y_x'; y_M]$.

4.2.2. NED algebraic transformation
By the same approach as in Section 4.2.1, but starting with the NED-formulated measurement model

$$\rho_j = \left|\left| p_{nb}^n - p_{nt}^n + R_b^n p_{bc_j}^b \right|\right| \tag{15}$$

a linear measurement model is found as

$$Y'_\chi = C'_{\chi,p}(z) p_{tb}^b \tag{16}$$

for the $M-1$ range difference measurements, where

$$Y'_\chi = \begin{bmatrix} \delta y_1 + \nu_{\chi,1}(z) \\ \vdots \\ \delta y_{M-1} + \nu_{\chi,M-1}(z) \end{bmatrix}, C'_{\chi,p}(z) = \begin{bmatrix} C_{\chi,1}(z) \\ \vdots \\ C_{\chi,M-1}(z) \end{bmatrix}$$

$$\nu_{\chi,j} = \frac{2 p_{nt}^{n\top} R_b^n \left(p_{bc_j}^b - p_{bc_M}^b \right) - \left|\left| p_{bc_j}^b \right|\right|^2 + \left|\left| p_{bc_M}^b \right|\right|^2}{\delta y_j + 2 y_M} \tag{17a}$$

$$C_{\chi,j}(z) = \frac{2 \left(R_b^n \left(p_{bc_j}^b - p_{bc_M}^b \right) \right)^\top}{\delta y_j + 2 y_M} \tag{17b}$$

From this, a position estimate $\check{p}_{nb}^n$ can be found, about which the range measurement model $h_M(\chi, z)$ is linearized:

$$\check{p}_{nb}^n = C'_{\chi,p}(\check{z})^\dagger Y'_\chi, \quad \check{\chi} = [\check{p}_{nb}^n; 0_{3\times 1}]$$

$$h_{\chi,M}(\chi, z) = h_{\chi,M}(\check{\chi}, z) + H_{\chi,M}(\check{\chi}, z)(\chi - \check{\chi}) + \overline{\varphi}_{\chi,M}\left(p_{nb}^n - \check{p}_{nb}^n \right)$$

$$H_{\chi,M}(\check{\chi}, z) = \begin{bmatrix} \dfrac{\check{p}_{nb}^n - p_{nt}^n + R_b^n p_{bc_j}^b}{\left|\left| \check{p}_{nb}^n - p_{nt}^n + R_b^n p_{bc_j}^b \right|\right|} & 0_{1\times 3} \end{bmatrix}$$

where $\overline{\varphi}_{\chi,M}\left(p_{nb}^n - \check{p}_{nb}^n \right)$ is higher order terms and $\overline{\varphi}_{\chi,M}(0) = 0$. Lastly, we define $C'_\chi(z) \triangleq [C'_{\chi,p}(z), \ 0_{M-1\times 3}]$, $C_\chi(\check{\chi}, \ z) \triangleq [C'_\chi(z); H_{\chi,M}(\check{\chi}, \ z)]$, and $Y_\chi \triangleq [Y'_\chi; y_M]$.

4.3. Stage 2: LTV KF

4.3.1. Body-fixed formulation

Denote by $\overline{x}$ the state estimate of the second stage body-fixed KF. We define the estimated measurement and find the measurement error

$$\overline{Y}_x \triangleq \begin{bmatrix} C'_x \overline{x} \\ h_M(\check{x}) + H_{x,M}(\check{x})(\overline{x} - \check{x}) \end{bmatrix}$$

$$\tilde{Y}_x = Y_x - \overline{Y}_x = C_x(\check{x})\widetilde{x} + \overline{\varphi}_x\left(p_{tb}^b - \check{p}_{tb}^b \right)$$

respectively, where $\widetilde{x} \triangleq x - \overline{x}$, $\overline{\varphi}_x(p) = [0_{M-1\times 1}; \overline{\varphi}_{x,M}(p)]$. Now, we define the estimator

$$\dot{\overline{x}} = A_x(t, \check{z})\overline{x} + B_x(\check{z})u + \overline{K}_x(t)\tilde{Y}_x \tag{18}$$

where $\overline{K}_x(t)$ is the solution of the Riccati equation inserted $A_x(t,\check{z})$, $C_x(\check{x})$, $G_x(\check{x})$, $\mathscr{C}_x = \mathrm{E}(\varepsilon_x \varepsilon_x^\top) = \mathrm{diag}(\sigma_{ars}^2 l_3, \sigma_{acc}^2 l_3)$. The elements of the measurement covariance matrix $\mathscr{R}$ are given by

$$\begin{aligned} \mathscr{R}_{i,j} = \mathrm{Cov}(\partial y_j, \partial y_i) &= \mathrm{E}\big[(\varepsilon_{\partial,j} - \varepsilon_{\partial,m})(\varepsilon_{\partial,i} - \varepsilon_{\partial,m}) \big] \\ &= \mathrm{E}(\varepsilon_{y,j}\varepsilon_{y,i}) + \mathrm{E}(\varepsilon_{y,m}\varepsilon_{y,m}) \\ &= \begin{cases} 2\sigma_\partial^2, & i = j \\ \sigma_\partial^2, & i \neq j \end{cases} \end{aligned} \tag{19a}$$

$$\begin{aligned} \mathscr{R}_{j,M} = \mathrm{Cov}(\partial y_j, y_M) &= \mathrm{E}\left[\left(\tfrac{1}{2}\varepsilon_y + \tfrac{1}{2}\varepsilon_{\partial,m} \right)(\varepsilon_{\partial,i} - \varepsilon_{\partial,m}) \right] \\ &= -\tfrac{1}{2}\sigma_\partial^2 \end{aligned} \tag{19b}$$

$$\begin{aligned} \mathscr{R}_{M,M} = \mathrm{Cov}(y_M, y_M) &= \mathrm{E}\left[\left(\tfrac{1}{2}\varepsilon_y + \tfrac{1}{2}\varepsilon_{\partial,m} \right)^2 \right] \\ &= \tfrac{1}{4}\left(\sigma_y^2 + \sigma_\partial^2 \right) \end{aligned} \tag{19c}$$

for $i,j \in (1,\ldots,M)$. Here, the noise terms in the denominator of $\nu_{x,j}$ and $C_{x,j}$ in (13) and (17) have been neglected. Assuming y_M dominates ∂y_j in the denominator, we approximate the noise characteristics of the term

$$\frac{1}{y_M} \approx \frac{1}{\rho_M + \varepsilon_M} = \frac{1}{\rho_M}\frac{1}{1 + \varepsilon_M/\rho_M} \approx \frac{1}{\rho_M}\left(1 - \frac{\varepsilon_M}{\rho_M} \right)$$

$$\approx \frac{1}{\rho_M} - \frac{\varepsilon_M}{\rho_M^2} \sim \mathcal{N}\left(1/\rho_M, \sigma_y^2 \big/ \rho_M^4 \right)$$

The effect of the noise in the denominators of (13) and (17a) can be assumed negligible if the transceiver baselines on the UV are short relative to the distance to the transponder. Without loss of generality, the origin of the NED coordinate frame can be set in the transponder, making $p_{nt}^n = 0$ in (17a). This justifies neglecting the noise terms in the denominators of (13) and (17).

Subtracting (18) from (9) yields the following nominal error dynamics in the noise-free case:

$$\Sigma_x : \dot{\widetilde{x}} = \left(A_x(t, \check{z}) - \overline{K}_x(t)C_x(\check{x}) \right)\widetilde{x} + \overline{\xi}_x\left(z, \check{z}, p_{tb}^b, \check{p}_{tb}^b \right) \tag{20}$$

where $\overline{\xi}_x(z, \check{z}, p_{tb}^b, \check{p}_{tb}^b) = (A_x(t, z) - A_x(t, \check{z}))x + (B_x(z) - B_x(\check{z})u(t)) + \overline{K}_x(t)\overline{\varphi}_x(p_{tb}^b - \check{p}_{tb}^b)$.

4.3.2. NED formulation

Denote by $\overline{\chi}$ the state estimate of the second stage NED KF and define the state error $\widetilde{\chi} \triangleq \chi - \overline{\chi}$. We define the estimated measurement and find the measurement error

$$\overline{Y}_\chi \triangleq \begin{bmatrix} C'_\chi(\check{z})\overline{\chi} \\ h(\check{\chi}, \check{z}) + H_{\chi,M}(\check{\chi}, \check{z})(\overline{\chi} - \check{\chi}) \end{bmatrix} \tag{21}$$

$$\tilde{Y}_\chi = Y_\chi - \overline{Y}_\chi = C_\chi(\check{\chi}, \check{z})\widetilde{\chi} + \overline{\xi}_{\chi,Y}(\chi, z, \check{\chi}, \check{z}) \tag{22}$$

respectively, where

$$\overline{\xi}_{\chi,Y}(\chi, z, \check{\chi}, \check{z}) = \left[\overline{\xi}'(\chi, z, \check{z}); \overline{\xi}_M(\chi, z, \check{\chi}, \check{z}) \right]$$

$$\overline{\xi}'(\chi, z, \check{z}) = \left(C_\chi(z) - C'_\chi(\check{z}) \right)\chi$$

$$\overline{\xi}_M(\chi, z, \check{\chi}, \check{z}) = h(\check{\chi}, z) - h(\check{\chi}, \check{z}) + \overline{\varphi}_{\chi,M}\left(p_{nb}^n - \check{p}_{nb}^n \right) + \left(H_{\chi,M}(\check{\chi}, z) - H_{\chi,M}(\check{\chi}, \check{z}) \right)(\chi - \check{\chi})$$

Now, we define the estimator

$$\dot{\overline{\chi}} = A_\chi \overline{\chi} + B_\chi(\check{z})u + \overline{K}_\chi(t)\overline{Y}_\chi \tag{23}$$

where $\overline{K}_\chi(t)$ is the solution of the Riccati equation inserted A_χ, $C_\chi(\check{\chi}, \check{z})$, $G_{\check{z}}(\check{\chi})$, $\mathscr{C}_\chi = \mathrm{E}(\varepsilon_\chi \varepsilon_\chi^\top) = I_3 \sigma_{acc}^2$, and the measurement covariance matrix $\mathscr{R}$ given by (19).

Subtracting (23) from (11) yields the following nominal error dynamics in the noise-free case

$$\overline{\Sigma}_\chi : \dot{\widetilde{\overline{\chi}}} = \left(A_\chi - \overline{K}_\chi(t)C_\chi(\check{\chi}, \check{z})\right)\widetilde{\overline{\chi}} + \overline{\xi}_\chi(\chi, z, \check{\chi}, \check{z}) \tag{24}$$

where

$$\overline{\xi}_\chi(\chi, z, \check{\chi}, \check{z}) = \overline{K}_\chi(t)\overline{\xi}_{\chi, Y}(\chi, z, \check{\chi}, \check{z}) + \left(B_\chi(z) - B_\chi(\check{z})\right)u(t)$$

4.4. Stage 3: linearized KF

4.4.1. Body-fixed formulation
Linearizing (4) about $\overline{x}$ yields

$$h_j(x) = h_j(\overline{x}) + H_{x,j}(\overline{x})\left(\widetilde{\overline{x}}\right) + \widehat{\varphi}_{x,j}\left(\widetilde{\overline{x}}\right)$$

$$H_{x,j}(\overline{x}) = \left[\frac{\left(\overline{p}_{tb}^b - p_{bc_j}^b\right)^\top}{\left\|\overline{p}_{tb}^b - p_{bc_j}^b\right\|} - \frac{\left(\overline{p}_{tb}^b - p_{bc_M}^b\right)^\top}{\left\|\overline{p}_{tb}^b - p_{bc_M}^b\right\|} \quad 0_{1\times 3} \right] \tag{25}$$

for $j \in (1, ..., M-1)$, where $\widehat{\varphi}_{x,j}(\widetilde{\overline{x}})$ contains higher order terms and $\widehat{\varphi}_{x,j}(0) = 0$. Concatenating (25) and a similar linearization of $h_M(x)$ yields

$$h(x) = h(\overline{x}) + H_x(\overline{x})\widetilde{\overline{x}} + \widehat{\varphi}_x\left(\widetilde{\overline{x}}\right) \tag{26}$$

where $H_x(\overline{x}) = [H_{x,1}(\overline{x}); ...; H_{x,M}(\overline{x})]$, $H_{x,M}(\overline{x})$ is given by (14), and $\widehat{\varphi}(\widetilde{\overline{x}}) = [\widehat{\varphi}_{x,1}(\widetilde{\overline{x}}); ...; \widehat{\varphi}_{x,M}(\widetilde{\overline{x}})]$. Now, defining $\widehat{y}_x \triangleq h(\overline{x}) + H_x(\overline{x})(\widehat{x} - \overline{x})$ yields the measurement error $\widetilde{y}_x \triangleq y - \widehat{y}_x = H_x(\overline{x})\widetilde{x} + \widehat{\varphi}_x(\widetilde{\overline{x}})$.

Denote by $\widehat{x}$ the state estimate of the third stage body-fixed KF. We now define the estimator

$$\dot{\widehat{x}} = A_x(t, \check{z})\widehat{x} + B_x(\check{z})u(t) + \widehat{K}_x(t)\widetilde{y}_x \tag{27}$$

where $\widehat{K}_x(t)$ is the solution of the Riccati equations inserted $A_x(t, \check{z})$, $H_x(\overline{x})$, $G_x(\overline{x})$, $\mathscr{C}_x$, and $\mathscr{R}$ from (19).

Define $\widetilde{x} \triangleq x - \widehat{x}$. Subtracting (27) from (9) in the noise-free case yields the error dynamics:

$$\widehat{\Sigma}_x : \dot{\widetilde{x}} = \left(A_x(\check{z}) - \widehat{K}_x(t)H_x(\overline{x})\right)\widetilde{x} + \widehat{\xi}_x(x, z, \overline{x}, \check{z}) \tag{28}$$

where

$$\widehat{\xi}_x(x, z, \overline{x}, \check{z}) = (A_x(z) - A_x(\check{z}))x + (B_x(z) - B_x(\check{z}))u(t) - \widehat{K}_x(t)\widehat{\varphi}_x\left(\widetilde{\overline{x}}\right)$$

4.4.2. NED formulation
We begin by linearizing (4) about $\overline{\chi}$:

$$h_j(\chi, z) = h_j(\overline{\chi}, z) + H_{\chi,j}(\overline{\chi}, z)\widetilde{\overline{\chi}} + \widehat{\varphi}_{\chi,j}\left(\widetilde{\overline{\chi}}\right)$$

where $H_{\chi,j}(\chi, z) = [H_{p\chi j}(\chi, z), 0_{1\times 3}]$,

$$H_{p\chi j}(\overline{\chi}, z) = \left[\frac{\left(\overline{p}_{nb}^n + R_b^n p_{bc_j}^b - p_{nt}^n\right)^\top}{\left\|\overline{p}_{nb}^n + R_b^n p_{bc_j}^b - p_{nt}^n\right\|} - \frac{\left(\overline{p}_{nb}^n + R_b^n p_{bc_m}^b - p_{nt}^n\right)^\top}{\left\|\overline{p}_{nb}^n + R_b^n p_{bc_m}^b - p_{nt}^n\right\|} \right]$$

$\widehat{\varphi}_{\chi j}(\widetilde{\overline{\chi}})$ is higher order terms, and $\widehat{\varphi}_{\chi j}(0) = 0$. Concatenating this and a

linearization of $h_M(\chi, z)$ yields

$$h(\chi, z) = h(\overline{\chi}, z) + H_\chi(\overline{\chi}, z)\widetilde{\overline{\chi}} + \widehat{\varphi}_\chi\left(\widetilde{\overline{\chi}}\right) \tag{29}$$

where $H_\chi(\overline{\chi}, z) = [H_{\chi,1}(\overline{\chi}, z); ...; H_{\chi,M}(\overline{\chi}, z)]$, $H_{\chi j} = [H_{p\chi j}, 0_{1\times 3}]$ for $j \in (1, ..., M-1)$, and $\widehat{\varphi}_\chi(\widetilde{\overline{\chi}}) = [\widehat{\varphi}_{\chi,1}(\widetilde{\overline{\chi}}); ...; \widehat{\varphi}_{\chi,M}(\widetilde{\overline{\chi}})]$.

Denote by $\widehat{\chi}$ the state estimate of the third stage NED KF and define the state error $\widetilde{\chi} \triangleq \chi - \widehat{\chi}$. Now, we define the estimated measurement

$$\widehat{y}_\chi \triangleq h(\overline{\chi}, \check{z}) + H(\overline{\chi}, \check{z})(\widehat{\chi} - \overline{\chi}) \tag{30}$$

and find the measurement error in the case noise-free case as

$$\widetilde{y}_\chi \triangleq y - \widehat{y}_\chi = H(\overline{\chi}, \check{z})\widetilde{\chi} + \widehat{\xi}_{\chi,y}(\chi, \overline{\chi}, z, \check{z}) \tag{31}$$

where

$$\widehat{\xi}_{\chi,y}(\chi, \overline{\chi}, z, \check{z}) = h(\overline{\chi}, z) - h(\overline{\chi}, \check{z}) + \widehat{\varphi}_x\left(\widetilde{\overline{\chi}}\right) + (H_x(\overline{\chi}, z) - H_x(\overline{\chi}, \check{z}))\widetilde{\overline{\chi}}$$

An estimator is defined

$$\dot{\widehat{\chi}} = A_\chi \widehat{\chi} + B_\chi(\check{z})u + \widehat{K}_\chi(t)\widetilde{y}_\chi \tag{32}$$

where $\widehat{K}_\chi(t)$ is the solution of the Riccati equation inserted $A_\chi(t, \check{z})$, $H_\chi(\check{\chi}, \check{z})$, $G_\chi(\check{\chi})$, $\mathscr{C}_\chi = \mathrm{E}(\varepsilon_\chi \varepsilon_\chi^\top) = I_3 \sigma_{acc}^2$, and the measurement covariance matrix $\mathscr{R}$ given by (19).

Lastly, the error dynamics is found by subtracting (32) from (11)

$$\widehat{\Sigma}_\chi : \dot{\widetilde{\chi}} = \left(A_\chi - \widehat{K}_\chi(t)H_\chi(\overline{\chi})\right)\widetilde{\chi} + \widehat{\xi}_\chi(\chi, \overline{\chi}, z, \check{z}) \tag{33}$$

where $\widehat{\xi}_\chi(\chi, \overline{\chi}, z, \check{z}) = \widehat{\xi}_{\chi,y}(\chi, \overline{\chi}, z, \check{z}) - \widehat{K}_\chi(t)\widehat{\varphi}_\chi(\widetilde{\overline{\chi}}) + (B_\chi(z) - B_\chi(\check{z}))u(t)$.

5. Stability analysis

The inputs $f_{nb,m}^b$ and $\omega_{nb,m}^b$ are assumed to be bounded.

Proposition 2 *The systems* $(A_x(\check{z}, t), C_x(\check{x}), G_x(\check{x}))$, $(A_\chi, C_\chi(\check{\chi}, \check{z}), G_\chi(\check{z}))$, $(A_x(\check{z}, t), C_x(\overline{x}), G_x(\overline{x}))$, *and* $(A_\chi, C_\chi(\check{\chi}, \check{z}), G_\chi(\check{z}))$ *are uniformly completely observable (UCO) and uniformly completely controllable (UCC).*

Proof. Theorem 6. O12 in Chen (1998) proves that the pairs $(A(t), D(t))$ is UCO if the observability co-distribution formed by $A(t)$ and $D(t)$ have full rank. We define the placeholder matrix $D(t) \in \{C_x(\check{x}), C_\chi(\check{\chi}, \check{z}), H_x(\overline{x}), H_\chi(\overline{\chi}, \check{z})\}$ and note its general form $D = [D_p(t), 0_{M\times 3}]$ where $D_p(t) \in \mathbb{R}^{M\times 3}$. The top $2M$ rows of the observability co-distributions are

$$\mathrm{d}\mathscr{O} = \begin{bmatrix} D_p(t) & 0_{M\times 3} \\ \star & D_p(t) \end{bmatrix} \tag{34}$$

where $\star$ denotes an arbitrary matrix of appropriate size. From Theorem 4.2 of Meyer (1973), it follows that if $D_p(t)$ has full rank, then $\mathrm{d}\mathscr{O}$ has full rank. The rank of $D_p(t)$ is full for all four systems under Assumption 2, and thus, all systems are UCO.

Using Theorem 6.12 in Chen (1998) in a similar way, it is trivial to show UCC of all four systems.

Since A_x, C_x, B_x, $\overline{\varphi}_x$ are smooth and z, $\check{z}$, p_{tb}^b, $\check{p}_{tb}^b$, u are bounded, there exists a constant $\overline{\alpha}_x > 0$ such that

$$\overline{\xi}_x\left(z, \check{z}, p_{tb}^b, \check{p}_{tb}^b\right) \leq \overline{\alpha}_x\left(\left\|p_{tb}^b - \check{p}_{tb}^b\right\|^2 + \|\check{z}\|^2\right) \tag{35}$$

Since B_χ, C'_χ, h, $H_{\chi,M}$, $\overline{\varphi}_{\chi,M}$ are smooth and z, $\check{z}$, χ, $\check{\chi}$, u are bounded, we know that there also exists a constant $\overline{\alpha}_\chi > 0$ such that

$$\bar{\xi}_\chi(\chi, z, \check{\chi}, \check{z}) \leq \bar{\alpha}_\chi\left(\left\|p_{nb}^n - \check{p}_{nb}^n\right\|^2 + \|\check{z}\|^2\right) \tag{36}$$

Notice that only the position and not the full state is used in the bounds (35)–(36) since the errors $\bar{\xi}_x$ and $\bar{\xi}_\chi$ do not depend on velocity.

Proposition 3 *Consider the nominal case with no noise, i.e., $\varepsilon_{ars} = \varepsilon_{acc} = 0, \varepsilon_y = 0, \varepsilon_{\partial,j} = 0, j \in (1, ..., M)$ and that the matrices $\mathcal{Q}_x$, $\mathcal{Q}_\chi$, $\mathcal{R}$, and $\mathcal{P}(0)$ are symmetric and positive definite.*

1. *The equilibrium points $\tilde{z} = (0, 0)$ and $\widetilde{\overline{x}} = 0$ of the error dynamics cascade Σ_z–$\overline{\Sigma}_x$ is GES.*

2. *The equilibrium points $\tilde{z} = (0, 0)$ and $\widetilde{\overline{\chi}} = 0$ of the error dynamics cascade Σ_z–$\overline{\Sigma}_\chi$ is GES.*

Proof. The proof uses similar arguments as Johansen and Fossen (2017).

Notice that in the noise-free case, we have $\check{p}_{tb}^b \equiv p_{tb}^b$ and $\check{p}_{nb}^n \equiv p_{nb}^n$. Furthermore, when $\check{z} = z$, then $\bar{\xi}_x = 0$ and $\bar{\xi}_\chi = 0$. Using Proposition 2, the equilibrium points $\widetilde{\overline{x}} = 0$ and $\widetilde{\overline{\chi}} = 0$ of the error dynamics $\overline{\Sigma}_x$ and $\overline{\Sigma}_\chi$, respectively, are GES as proven Anderson (1971). When $\check{z} \neq z$, $\bar{\xi}_x$ and $\bar{\xi}_\chi$ are bounded by (35) and (36), respectively. Proposition 1, Theorem 2.1 and Proposition 2.3 of Loria and Panteley (2005) now proves that the equilibrium points $\tilde{z} = (0, 0)$ and $\widetilde{\overline{x}} = 0$ and $\widetilde{\overline{\chi}} = 0$ of the error dynamics cascades Σ_z–$\overline{\Sigma}_x$ and Σ_z–$\overline{\Sigma}_\chi$, respectively, are GES. ∎

From Proposition 3, it follows that $\overline{x}$ and $\overline{\chi}$ are bounded.

Since $A_x, B_x, \widehat{\varphi}_x$ are smooth and $x, \overline{x}, z, \check{z}, u$ are bounded, there exists a constant $\widehat{\alpha}_x > 0$ such that

$$\widehat{\xi}_x(x, z, \overline{x}, \check{z}) \leq \widehat{\alpha}_x\left(\left\|\widetilde{\overline{x}}\right\|^2 + \|\check{z}\|^2\right) \tag{37}$$

Since $B_\chi, h, H_\chi, \widehat{\varphi}_\chi$ are smooth and $\chi, \overline{\chi}, z, \check{z}, u$ are bounded, there exists a constant $\widehat{\alpha}_\chi > 0$ such that

$$\widehat{\xi}_\chi(\chi, z, \overline{\chi}, \check{z}) \leq \widehat{\alpha}_\chi\left(\left\|\widetilde{\overline{\chi}}\right\|^2 + \|\check{z}\|^2\right) \tag{38}$$

Proposition 4 *Consider the nominal case with no noise, i.e., $\varepsilon_{ars} = \varepsilon_{acc} = 0, \varepsilon_y = 0, \varepsilon_{\partial,j} = 0, j \in (1, ..., M)$, and that the matrices $\mathcal{Q}_x$, $\mathcal{Q}_\chi$, $\mathcal{R}$, and $\mathcal{P}(0)$ are symmetric and positive definite.*

1. *The equilibrium points $\tilde{z} = (0, 0)$, $\widetilde{\overline{x}} = 0$, and $\hat{x} = 0$ of the error dynamics cascade Σ_z–$\overline{\Sigma}_x$–$\widehat{\Sigma}_x$ is GES.*

2. *The equilibrium points $\tilde{z} = (0, 0)$, $\widetilde{\overline{\chi}} = 0$, and $\hat{\chi} = 0$ of the error dynamics cascade Σ_z–$\overline{\Sigma}_\chi$–$\widehat{\Sigma}_\chi$ is GES.*

Proof. The proof is similar to that of Proposition 3.

6. Results

In this section, the results of simulations and experiments are shown. A depth measurement, modeled by

$$y_d = p_{nt,3}^n + \underbrace{\begin{bmatrix} R_{b,3}^n & 0_{1\times3} \end{bmatrix}}_{c_d^b(\check{z})} x = \underbrace{\begin{bmatrix} 0 & 0 & 1 & 0_{1\times3} \end{bmatrix}}_{C_d^n} \chi \tag{39}$$

where $R_{b,3}^n$ and $p_{nt,3}^n$ are the third rows of R_b^n and p_{nt}^n, respectively, is added to the filters by appending y_d to y, C_d^b to C_x and H_x, and C_d^n to C_χ and H_χ. It can be shown that this relaxes Assumption 2 to minimum 3 non-collinear receivers that construct minimally 2 non-vertical baselines.

In the implementation of the filters, some practical considerations were taken:
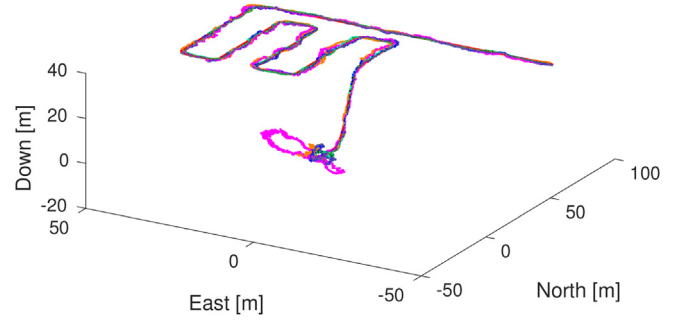

Fig. 3. The simulated trajectory and estimates in one of the simulations.

- $-S(p_{tb}^b)$ and $-S(v_{nb}^b)$ were removed from $G_x(x)$ since they greatly deteriorated the estimation. This is assumed to be caused by errors in the estimate of p_{tb}^b leading to an erroneous increase in the covariance matrix over time. Since p_{tb}^b typically is large, this may have a detrimental effect on estimation.
- For the body-fixed filters, the depth measurement variance was increased by a factor of 100, i.e. $\mathcal{R}_d = 100\sigma_d^2$. This accounted for the impact of small errors in R_b^n, which was amplified by the distance to the transponder, as can be seen in (39).

In the plots below, the following color coding is used:

1. Red — True or camera system trajectory
2. Pink — Stage 1 and 2 from Stovner and Johansen (2017).
3. Blue — Body-fixed stage 2 filter (18)
4. Cyan — NED stage 2 filter (23)
5. Grey — Loosely coupled NED filter
6. Orange — Body-fixed stage 3 filter (27)
7. Green — NED stage 3 filter (32)
8. Black — EKF based on NED formulation

The loosely coupled filter 5 is a NED formulated filter with the measurement model $\check{p}_{nb}^n = C\chi$, where $C = [I_3, 0_{3\times3}]$.

6.1. Simulations

The simulations were conducted with three different transponder positions in order to show how the estimators perform with increasing range measurements. In each of the three simulated scenarios, 50 simulations were run with different randomly generated noise. In the 800 s long scenario, the UV stood still for 400 s before following the trajectory shown in Fig. 3.

The transponder was placed at $p_{nt}^n = [-10, -20, 5]m$, $p_{nt}^n = [-100, -200, 50]m$, and $p_{nt}^n = [-1000, -2000, 50]m$ in the three scenarios, while the $M = 4$ receivers on the body were at

$$p_{bc_1}^b = [0.6, 0.3, -0.3]m, \; p_{bc_2}^b = [0.6, -0.3, 0.3]m$$

$$p_{bc_3}^b = [-0.6, 0.3, 0.3]m, \; p_{bc_4}^b = [-0.6, -0.3, -0.3]m$$

where $p_{bc_4}^b$ was also the position of the sender.

The initial state of the vehicle was given by $p_{nb}^n = [0, 0, 0]m$, $v_{nb}^n = [0, 0, 0]m/s$, $R_b^n = I_3$, while the ARS bias was $b^b = [0.012, -0.021, 0.014]rad/s$. The standard deviations of the measurement noises were $\sigma_y = 1m$, $\sigma_\partial = 0.01m$, $\sigma_d = 0.1m$, $\sigma_{acc} = 0.01m/s^2$, $\sigma_{ars} = 0.01rad/s$, and $\sigma_{mag} = 0.01$. The reference vectors used for attitude estimation were $r_1^n = g^n$, $r_1^b = f_{nb,m}^b$, $r_2^n = m^n = [1, 0, 0]$, and $r_2^b = m^b$. The frequency of acoustic, depth, and IMU measurement retrieval were $1Hz$, $10Hz$, and $100Hz$, respectively.
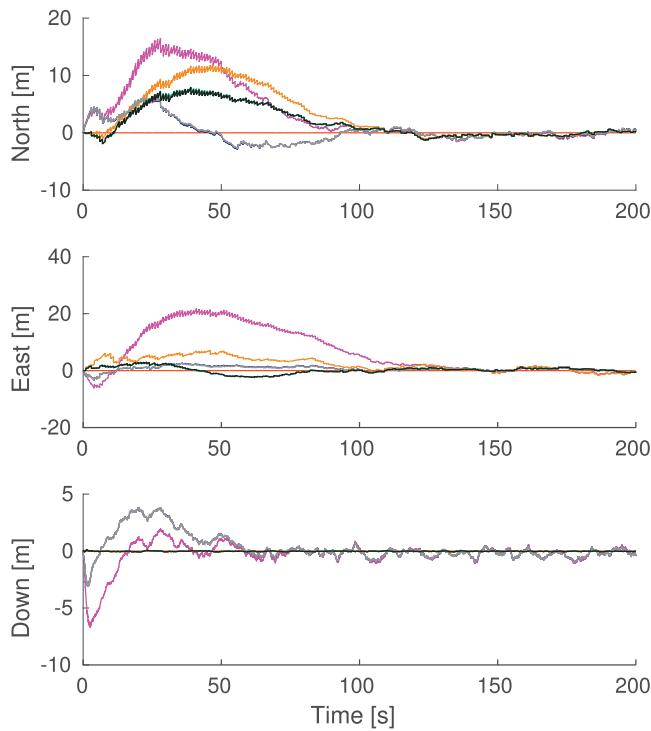
Fig. 4. The transient of the NED position estimation errors in one of the simulations. The black, green, and cyan curves are overlapping, and so are the gray and blue. (For interpretation of the references to color in this figure legend, the reader is referred to the Web version of this article.)

Fig. 5. The sensor platform with hydroacoustic transducers (on rods), Qualisys markers (reflective balls), and an underwater housing. The blue light is emitted from the OQUS camera system in order to better detect the reflective markers. (For interpretation of the references to color in this figure legend, the reader is referred to the Web version of this article.)

Table 1
MAE values in the last 400 s of simulation in the cases where distance to the transponder was short (s), medium (m), and long (l).

Est.	XY s [m]	Z s [m]	XY m [m]	Z m [m]	XY l [m]	Z l [m]
2)	0.095	0.240	0.226	0.254	15.437	0.406
3)	0.090	0.235	0.211	0.252	1.753	0.365
4)	0.082	0.025	0.194	0.025	0.848	0.025
5)	0.070	0.025	0.234	0.025	1.571	0.025
6)	0.087	0.236	0.200	0.251	1.735	0.365
7)	0.078	0.025	0.177	0.025	0.718	0.025
8)	0.078	0.025	0.176	0.025	0.718	0.025

The initial position, velocity, attitude, and bias estimates were $\hat{p}_{nb}^n(0) = [0,0,0]m$, $\hat{v}_{nb}^n(0) = [0,0,0]m/s$, $R_b^n(0) = I_3$, and $\hat{b}^b(0) = [0,0,0]rad/s$, from which the initial state of all estimators were found. The initial covariance matrix were chosen as $P(0) = \text{blockdiag}(I_3, 0.1I_3)$, where blockdiag($\cdot$) forms a block-diagonal matrix of its inputs. Choices for the attitude observer tuning parameters were $k_I = 0.05$, $\sigma = 1$, and $K_p = 1$. All estimators were updated with $100Hz$.

The difficult geometry of this estimation problem, i.e. the short baselines between receivers compared to the distance to transponder, makes this set up sensitive to noise on the acoustic measurements. This calls for conservative measurement updates in the KF. This can be seen by the slow convergence of the estimators in Fig. 4, which is seen to take approximately 100 s for all estimators even with no initial errors apart from the ARS bias. Little of the slow convergence can be attributed to the initial ARS bias error, since the NED and body-fixed filters converge with approximately the same speeds. Rather, this is due to the convergence of the covariance matrix.

In Table 1, the MAE of the horizontal (XY) and vertical (Z) positions for the last 400 s of simulations of the three scenarios are shown. The increasing horizontal MAE with increasing distance to transponder is evidence that the noise sensitivity increases with distance as well. The

vertical errors, however, vary less with distance. The NED formulated filters 4, 5, 7, and 8 have constant vertical MAE, while the body-fixed filters 2, 3, and 6 increase somewhat. Moreover, the vertical errors are more that 10 times higher for the body-fixed filters than the NED filters. This is due to the noisy rotation matrix in (39), which has a detrimental effect on the depth measurements. One can draw the conclusion that the NED filters generally outperform the body-fixed filters both in vertical and horizontal performance. Looking at the NED formulated filters only, we see that the loosely coupled filter 5 performs substantially worse than the others. This is due to the highly noise sensitive calculation of $\hat{p}_{nb}^n$, and speaks for the benefit of using a tightly coupled filter scheme. Filter 4 has somewhat higher MAE than the linearization based filters 7 and 8. Compared to filter 7, it only has half the computational complexity since it employs one KF instead of two, and compared to filter 8, it has guaranteed stability. Therefore, it is argued that filter 4 yields the best compromise between computational load, stability, and performance. This is especially true in the suggested case where the UV is far away from infrastructure and the highest precision of estimation is not crucial.

Filter 7 and 8 have similar performances, which is expected as filter 8 is just an EKF version of filter 7.

In this simulation study, it was assumed that the range measurement was retrieved instantaneously, and not influenced by the travel time of the sound wave. This assumption was made for simplicity. In a realistic scenario, especially when the vehicle is far from the transponder, this should be taken into account.

6.2. Experiments

The experiment was conducted in the Marine Cybernetic Laboratory (MCLab), which is a water tank at NTNU. The MCLab is equipped with an OQUS Underwater camera positioning system from Qualisys providing reference position and attitude trajectories.

The experimental set up was slightly different than in the simulations, described below:

- The IMU used in the experiments, an ADIS16485, does not contain a magnetometer. Therefore, measurements from 3 additional transponders was used in order to provide yaw information to the attitude estimator. Also, for ease of implementation, a standard multiplicative extended Kalman filter (MEKF) was employed, using accelerometer and the acoustics as reference vector measurements.
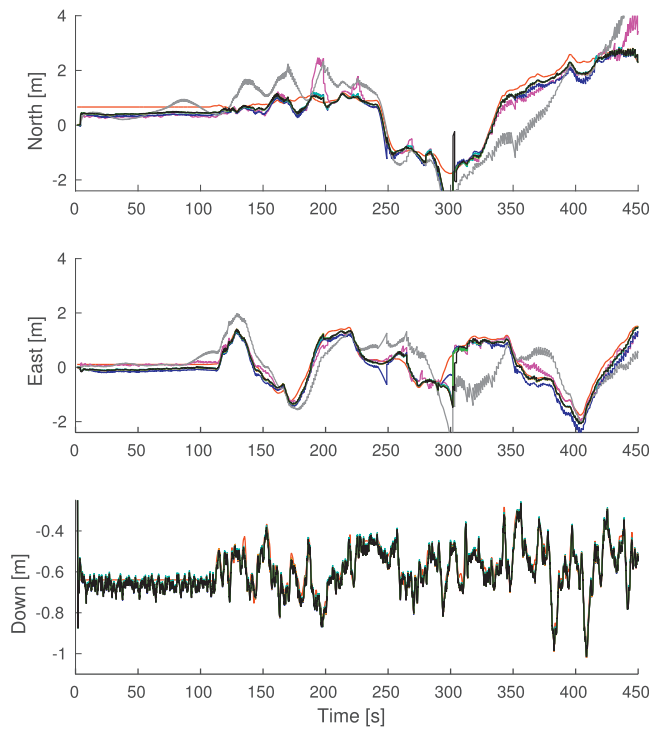
Fig. 6. NED position estimates from experimental data.

Table 2
MAE values from the experiments.

Est.	XY [m]	Z [m]
2)	0.3979	0.0269
3)	0.4030	0.0274
4)	0.2746	0.0232
5)	0.9384	0.0266
6)	0.2734	0.0269
7)	0.2702	0.0266
8)	0.2763	0.0266

- No pressure sensor was available, so the vertical position output from the Qualisys camera system was used instead. Onto this signal, a white noise $w_d \sim \mathcal{N}(0, 0.05^2)$ was added.
- The acoustic system provided range measurements. From this, range difference measurements were calculated by subtraction. Simple outlier rejection was employed to prevent corruption of the estimates.

The sensor platform was a $0.5 \times 0.5 \times 0.5m$ aluminum frame onto which an underwater housing containing an IMU was fastened, seen in Fig. 5. The transceiver positions were

$$p^b_{bc_1} = [0.78, 0.27, 0.26]m, \ p^b_{bc_2} = [0.45, -0.58, -0.28]m$$

$$p^b_{bc_3} = [-0.44, -0.23, 0.16]m, \ p^b_{bc_4} = [-0.44, 0.27, -0.25]m$$

and the transponder position $p^n_{nt} = [-2.11, 1.92, -0.76]m$. Acoustic measurements were retrieved with $1Hz$, while IMU and depth measurements were retrieved with $100Hz$ and $5Hz$, respectively. The tuning parameter standard deviations of the 3SFs and MEKF were $\sigma_y = 0.2m$, $\sigma_\partial = 0.1m$, $\sigma_{acc} = 0.034m/s^2$, $\sigma_{ars} = 0.0021rad/s$, and $\sigma_{\Delta p} = 0.1m$, where $\sigma_{\Delta p}$ represents the noise of the acoustic reference vector measurement used for the MEKF discussed above. The initial ARS bias estimate in the experiments was set to the values found by offline calibration.

From Fig. 6, we see that all filters except the loosely coupled filter 5 successfully tracked the true trajectory except about 300 s into the
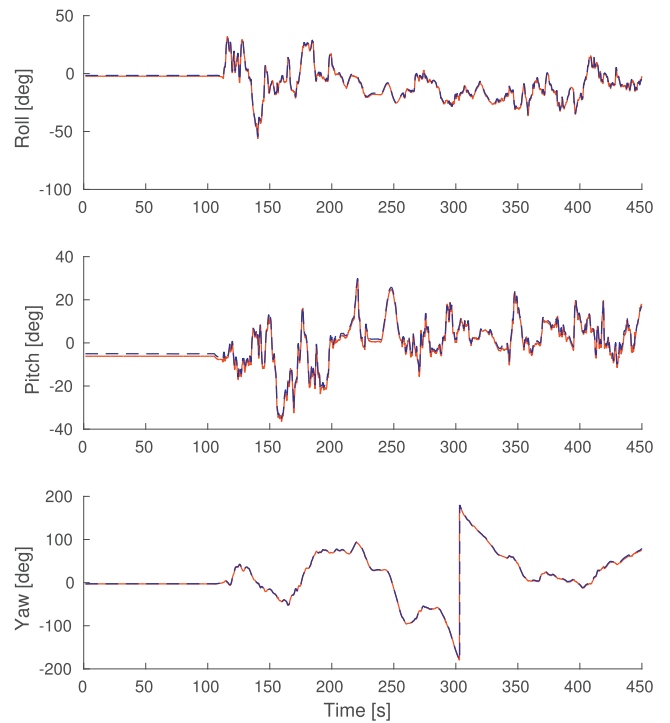

Fig. 7. Euler angles in experiments. The red curve is the ground truth trajectory from the camera system, and the blue dashed line is the MEKF estimate. (For interpretation of the references to color in this figure legend, the reader is referred to the Web version of this article.)
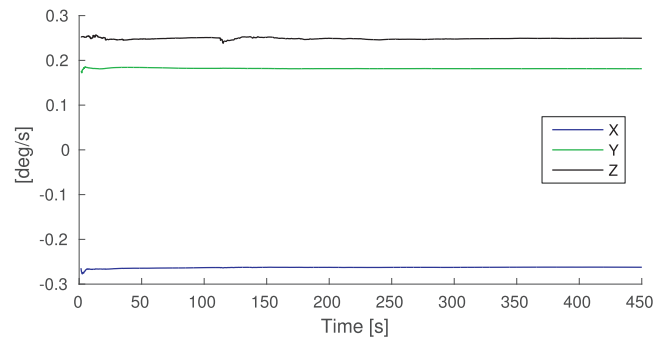

Fig. 8. ARS bias in experiments.

experiments. This was due to range measurement dropouts which resulted in a period of dead-reckoning. It is likely that filter 5 struggled because of small undetected outliers that greatly affected the noise sensitive calculation of $\hat{p}^n_{nb}$. Table 2 suggests that the body-fixed stage 2 filters, i.e. filter 2 and 3, perform worse than the NED stage 2 filter, i.e. filter 4. This confirms the conclusion drawn from the simulation study. Also, filter 4 performs equally well as the linearized filters, i.e. filter 6–8. This was also seen in the simulation study. Here, however, the distance between vehicle and transponder was much shorter than in the simulation study. This indicates that neglecting the noise terms in the denominators of (17) is justified also for short distances. That the performance of the body-fixed and NED linearized filters were similar, was expected, as the distance to the transponder was small. Figs. 7 and 8 show satisfying attitude and ARS bias estimation in the experiments.

7. Conclusion

In this paper, two novel GES 3SFs for underwater position estimation

using IMU, iSBL, and depth measurements was presented. These employed nonlinear transformations of the hydroacoustic measurement equations that yielded measurement equations on LTV forms. KFs were implemented using these LTV forms, which constituted the second stage of two new 3SFs. Based on the estimates from these, third stage linearized filters were implemented.

A comparison study between several KFs based on NED and body-fixed formulations were conducted. Generally, it was found that the NED formulated filters performed better than the body-fixed ones. This was likely due to that the NED formulated filters are better incorporating depth measurements and have a lower sensitivity to noisy attitude and ARS bias estimates. Specifically, the novel second stage filter employing the NED formulation showed the most promise at it performed nearly as well as its purely linearization-based third stage filter and EKF counterparts while leaving half the computational footprint of the full 3SF and guaranteeing global stability in contrast to the local stability of the EKF.

Future work should include a comparison study with the other contributors to this estimation problem, especially Morgado et al. (2011b, 2013); Batista et al. (2014).

Acknowledgments

References

Anderson, B.D.O., 1971. Stability properties of kalman-Bucy filters. J. Franklin Inst. 291 (2), 137–144.

Bancroft, S., 1985. An algebraic solution of the GPS equations. IEEE Transactions on Aerospace and Electronic Systems AES 21 (1), 56–59.

Batista, P., Silvestre, C., Oliveira, P., 2010. Single beacon navigation: observability analysis and filter design. American Control Conference (ACC) 2010, 6191–6196.

Batista, P., Silvestre, C., Oliveira, P., 2012. GES integrated LBL/USBL navigation system for underwater vehicles. Decis. Contr. 6609–6614.

Batista, P., Silvestre, C., Oliveira, P., 2014. Tightly coupled long baseline/ultra-short baseline integrated navigation system. Int. J. Syst. Sci. 47 (8), 1837–1855.

Chaffee, J., Abel, J., 1994. On the exact solutions of pseudorange equations. IEEE Trans. Aero. Electron. Syst. 30 (4), 1021–1030.

Chen, C., 1998. Linear System Theory and Design, third ed. Oxford University Press, Inc.

Ferreira, B., Matos, A., Cruz, N., sep 2010. Single beacon navigation: localization and control of the MARES AUV. In: OCEANS 2010 MTS. IEEE, pp. 1–9.

Grip, H.F., Fossen, T.I., Johansen, T.A., Saberi, A., 2015. Globally exponentially stable attitude and gyro bias estimation with application to GNSS/INS integration. Automatica 51, 158–166 (June).

Johansen, T.A., Fossen, T.I., 2017. The eXogenous kalman filter (XKF). Int. J. Contr. 90, 161–167.

Johansen, T.A., Fossen, T.I., Goodwin, G.C., 2016. Three-stage filter for position estimation using pseudo-range measurements. IEEE Trans. Aero. Electron. Syst. 1–12.

Jørgensen, E.K., Johansen, T.A., Schjølberg, I., 2016. Enhanced hydroacoustic range robustness of three-stage position filter based on long baseline measurements with unknown wave speed. In: Conference on Control Applications in Marine Systems.

Loria, A., Panteley, E., 2005. Cascaded nonlinear time-varying systems : analysis and design. In: Advanced Topics in Control Systems Theory. Springer, pp. 23–64. Ch. 2.

Meyer, C.D., 1973. Generalized inverses and ranks of block matrices. SIAM Rev. 25 (4), 597–602.

Morgado, M., Batista, P., Oliveira, P., Silvestre, C., 2011a. Position and Velocity USBL/IMU Sensor-based Navigation Filter, 18th IFAC World Congress, pp. 13642–13647.

Morgado, M., Batista, P., Oliveira, P., Silvestre, C., 2011b. Position USBL/DVL sensor-based navigation filter in the presence of unknown ocean currents. Automatica 47, 2604–2614.

Morgado, M., Oliveira, P., Silvestre, C., Jan 2013. Tightly coupled ultrashort baseline and inertial navigation system for underwater vehicles: an experimental validation. J. Field Robot. 30 (1), 142–170.

Saúde, J., Aguiar, A.P., Jan 2009. Single Beacon Acoustic Navigation for an AUV in the presence of unknown ocean currents. IFAC Proceedings Volumes 42 (18), 298–303.

Schjølberg, I., Gjersvik, T.B., Transeth, A.A., Utne, I.B., Jan 2016. Next generation subsea inspection, maintenance and repair operations. IFAC-PapersOnLine 49 (23), 434–439.

Stovner, B.B., Johansen, T.A., 2017. Hydroacoustically aided inertial navigation for joint position and attitude estimation in absence of magnetic field measurements. Proc. Am. Contr. Conf. 37 (1), 1211–1218.

Stovner, B.B., Johansen, T.A., Fossen, T.I., Schjølberg, I., 2016. Three-stage filter for position and velocity estimation from long baseline measurements with unknown wave speed. In: Proc. Of the American Contr. Conf, pp. 4532–4538.

Stovner, B.B., Johansen, T.A., Schjølberg, I., 2017. Globally exponentially stable aided inertial navigation with hydroacoustic measurements from one transponder. Proc. Am. Contr. Conf. 37 (1), 1219–1226.

Vickery, K., 1998. Acoustic Positioning Systems. A Practical Overview of Current Systems. Proceedings of the 1998 Workshop on Autonomous Underwater Vehicles (Cat. No.98CH36290), pp. 5–17.